Journal of Biomedical Optics 5(3), 277–282 (July 2000)

# Modeling photon transport in transabdominal fetal oximetry

**Steven L. Jacques**
Oregon Medical Laser Center
Portland, Oregon 97225

**Nimmi Ramanujam**
**Gargi Vishnoi**
**Regine Choe**
**Britton Chance**
University of Pennsylvania
Philadelphia, Pennsylvania 19104

**Abstract.** The possibility of optical oximetry of the blood in the fetal brain measured across the maternal abdomen just prior to birth is under investigation. Such measurements could detect fetal distress prior to birth and aid in the clinical decision regarding Cesarean section. This paper uses a perturbation method to model photon transport through an 8-cm-diam fetal brain located at a constant 2.5 cm below a curved maternal abdominal surface with an air/tissue boundary. In the simulation, a near-infrared light source delivers light to the abdomen and a detector is positioned up to 10 cm from the source along the arc of the abdominal surface. The light transport [W/cm$^2$ fluence rate per W incident power] collected at the 10 cm position is $T_m = 2.2\times10^{-6}$ cm$^{-2}$ if the fetal brain has the same optical properties as the mother and $T_f = 1.0\times10^{-6}$ cm$^{-2}$ for an optically perturbing fetal brain with typical brain optical properties. The perturbation $P=(T_f - T_m)/T_m$ is −53% due to the fetal brain. The model illustrates the challenge and feasibility of transabdominal oximetry of the fetal brain.
 [S1083-3668(00)01303-4]

Keywords: oximetry; fetal brain; optical transport; optical diagnostics.

Paper JBO-021 received Nov. 30, 1999; revised manuscript received Apr. 28, 2000; accepted for publication May 12, 2000.

## 1 Introduction

The possibility of optical oximetry of the blood in the fetal brain measured across the maternal abdomen just prior to birth is being investigated by Ramanujam et al.[1] Such measurements could detect fetal distress prior to birth and aid in the clinical decision regarding Cesarean section. This paper uses a perturbation method to estimate the perturbing signal expected from the fetal brain compared to the magnitude of the optical signal detected in such transabdominal measurements.

Previous work has outlined the use of the perturbation method to calculate fluence rate $(F)$(W/cm$^2$) distributions in a tissue with homogenous background optical properties and an embedded object with differing optical properties.[2–6] In this paper, the fetal brain is first treated as a single spherical object within an infinite homogeneous maternal tissue, then the air/tissue boundary at the abdominal surface is added to assess its influence on the problem. A simulated light source and detector are placed at positions that would be on the surface of the maternal abdomen. The results are reported as the transport factor $(T=F/S_0)$ (cm$^{-2}$) which equals the fluence rate $(F)$ (W/cm$^2$) per unit power of the source $(S_0)$ (W). The modeling is done using optical properties at a wavelength of 800 nm and illustrates typical near-infrared measurements. Multiple wavelength measurements would be combined to achieve transabdominal oximetry.

Address all correspondence to S. L. Jacques. Tel: 503-216-4092; Fax: 503-216-2422; e-mail: sjacques@ece.ogi.edu

## 2 Materials and Methods

### 2.1 Optical Properties and Geometry of Tissues

The optical properties used in this paper are for near-infrared wavelengths in the 700–900 nm range where oximetry is conducted due to the good light penetration through tissue and the sensitive oxygenation dependence of hemoglobin absorption. The background maternal tissues were assumed to have the following typical soft tissue optical properties: absorption coefficient $\mu_{am}$ equal to 0.08 cm$^{-1}$ and reduced scattering coefficient $\mu'_{sm}$ equal to 4 cm$^{-1}$. The fetal brain optical absorption coefficient $\mu_{af}$ is expected to vary between 0.10 and 0.15 cm$^{-1}$ and a mean value of 0.125 cm$^{-1}$ was used in the calculations. The incremental absorption of the fetal brain is $\Delta\mu_{af}=\mu_{af}-\mu_{am}=(0.125-0.08)=0.045$ cm$^{-1}$. The fetal scattering was assumed to equal the maternal scattering, $\mu'_{sf}=\mu'_{sm}$. Combining these optical properties for fetal brain yields an effective fetal attenuation coefficient, $\mu_{eff\,fetal}=[3\mu_{af}(\mu_{af}+\mu'_{sf})]^{1/2}$, of 1.24 cm$^{-1}$ which is consistent with the post-mortem *in situ* fetal brain optical properties reported by Svaasand et al. to be about 1–3 cm$^{-1}$ in the 660–1064 nm range.[7] Although Ostermeyer and Jacques[6] outline how to consider embedded objects with scattering properties that differ from the background, the treatment here would add complexity with only minor improvement in the lessons of this simple preliminary model. More important are the variation in thickness of the maternal tissue layer overlying the fetal brain and the influence of the amniotic fluid at the sides of the fetal head. Such issues are left to future work and are considered by Ramanujam[8] and Vishnoi.[9] In summary, the model as-

1083-3668/2000/$15.00 © 2000 SPIE

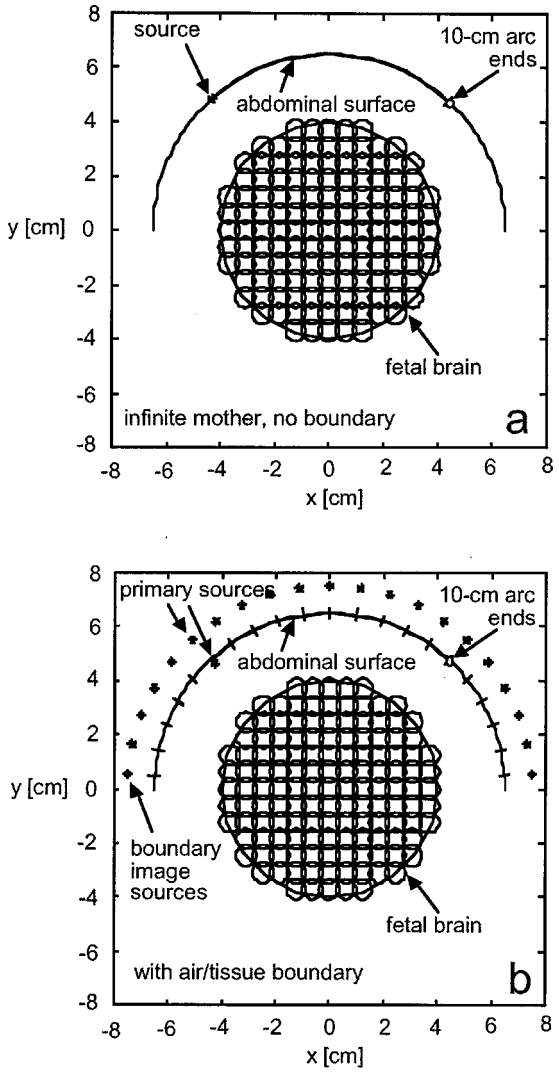


**Fig. 1** Model of fetal brain within maternal tissue. A 10 cm arc shows the location of the abdominal surface. An 8 cm diameter fetal brain is located 2.5 cm below the abdominal surface. Optical properties at 800 nm wavelength are $\mu'_{sm}=8\ cm^{-1}$, $\mu_{am}=0.08\ cm^{-1}$ for mother and $\mu'_{sf}=8\ cm^{-1}$, $\mu_{af}=0.125\ cm^{-1}$ for fetal brain. (a) No air/tissue boundary. (b) With air/tissue boundary, using a hemispherical distribution of image sources outside the abdominal surface within an infinite maternal tissue to mimic the air/tissue boundary. Some of the boundary images sources are shown.

sumes the maternal and fetal tissues have the same scattering properties but different absorption properties to approximate the clinical situation.

The geometry of the model is shown in Figure 1. An 8-cm-diam spherical fetal brain is centered at the origin ($x=0$, $y=0$, $z=0$). Only the results in the $x$-$y$ plane at $z=0$ which connects the source, fetal brain center, and detector are shown in Figure 1 but the model is three-dimensional. The maternal abdominal surface was located a constant 2.5 cm above the fetal brain. In reality, this maternal thickness probably increases toward the sides of the abdomen. In Figure 1(a), the infinite-mother model is shown where there is not an air/tissue interface at the abdominal surface. The source is at a position 44° to the left of the central plane through the abdomen, and the detector is at variable positions up to 44° to the right. In Figure 1(b), the air/tissue boundary at the abdominal surface is included, accomplished by treating the primary source as a pair of sources of equal magnitude, one positive just below the surface and one negative above the surface, and placing a hemispherical distribution of virtual boundary sources outside the abdominal surface whose magnitudes were adjusted to achieve the boundary condition relating fluence rate and outward flux at the surface. A 10-cm-long arc is shown in Figure 1 to indicate the locus of detector positions along the abdominal surface. In Figure 1(a), the source was located at the start of the arc at $x=-4.43$ cm, $y=4.76$ cm, $z=0$. In Figure 1(b), the positive source was placed one transport mean free path, $mfp'=1/(\mu_{am}+\mu'_{sm})$ (cm), below the above $(x,y,z)$ position on the surface, and a negative image source was placed a distance $mfp'+4AD$ above the surface. The factor $A$ equals $(1+r_{tir})/(1-r_{tir})$ where $r_{tir}$ is the total internal reflectance (equals 0.51) at the air/tissue boundary expected for a tissue with refractive index 1.37. The factor $D$ is the diffusion length equal to $mfp'/3$. The detector was moved along the arc to show how the transport signal varies with source-detector separation. The final detector position at the end of the 10 cm arc was $x=4.61$ cm, $y=4.58$ cm, $z=0$, which is a 9.04 cm direct distance from the source through the tissues.

The fetal brain was treated as the superposition of many small spherical volumes such that the total volume of the brain was conserved. The spheres overlap because they conserve total volume. The overlap volume corrects for the void volumes between spheres. Each small sphere had the optical properties of the fetal brain. There were 1189 spheres each with a diameter of 3.78 mm. The centers of the spheres were placed on a cubic grid of equal $x$, $y$, and $z$ spacings of 3.50 mm. The voxels do not exactly match the smooth spherical surface of the fetal brain but rather present a surface that is rough on the scale of the grid size. Such approximate resolution of the brain surface does not seriously compromise the calculations.

## 2.2 Perturbation Model: Infinite Mother With no Boundary

First, we consider the case of an infinite maternal tissue with no boundary [Figure 1(a)]. The use of perturbation methods is widely known and one implementation is used here.[5,6] This paper used diffusion theory to implement the model although the perturbation method can use other transport models such as Monte Carlo. The light source was treated as an isotropic point source of continuous light, $S_0$ (W), located at a position which would be on the maternal abdominal surface. The fetal brain was subdivided into the 1189 absorbing spherical volumes mentioned before. In general, the fluence rate $F_{ij}$ reaching the $i$th sphere in response to a $j$th source $S_j$ was calculated by the spherical point spread function of diffusion theory:

$$F_{ij}=S_jT_{ij}=S_j\frac{\exp(-\mu_{eff}r_{ij})}{4\pi Dr_{ij}}, \qquad (1)$$

where $r_{ij}$ is the distance between the $j$th source and the $i$th sphere. The transport factor $T_{ij}\,(cm^{-2})$ equals $F_{ij}/S_j$. The

diffusion length $D$ equals $1/[3(\mu_{am}+\mu'_{sm})]$. The effective maternal attenuation coefficient $\mu_{eff}$ equals $[3\mu_{am}(\mu_{am}+\mu'_{sm})]^{1/2}$ or $(\mu_{am}/D)^{1/2}$.

One can apply Eq. (1) for the case of $j=0$ to generate the $F_{i0}$ value at each $i$th sphere in response to the one primary source $S_0$. Such a calculation is called the Born approximation and ignores the influence of all the neighboring spheres on the ability of source light to transport to a particular sphere. The resulting fluence rate $F_{i0}$ at the $i$th sphere of volume $V$ ($cm^3$) and incremental absorption $\Delta\mu_{af}$ ($cm^{-1}$) undergoes an incremental absorption above the normal background tissue's absorption process. This incremental deposition of power acts as a negative source of light, $S_i$ (W), since it is a region in which light is removed from the tissue

$$S_i=-F_{ij}\Delta\mu_{af}V. \tag{2}$$

Consequently, each sphere acts as a virtual source of negative power that generates a negative field of light. Superposition of the positive fluence rate from the single primary source, $S_0$, and the negative fluence rate from all the virtual sources, $S_i$, yields the net fluence rate at any $i$th sphere

$$F_i=\sum_{j=0}^{N} S_jT_{ij}. \tag{3}$$

For the special case of the transport from an $i$th virtual source to itself, i.e., how does the incremental absorption of a sphere influence its own local fluence rate, the following transport factor $T_{ii}$ was used:[6]

$$T_{ii}=\frac{3}{4\pi\mu_{am}a^3}[1-(1+\mu_{eff}a)\exp(-\mu_{eff}a)], \tag{4}$$

where $a$ was the radius of an absorbing object ($a=1.89$ mm). Next, each $j$th virtual source was updated

$$S_j=-F_i\Delta\mu_{af}V, \tag{5}$$

where $j=i$, for all $i$th spheres.

In using Eqs. (3) and (5) to compute the virtual source powers, the values of all the virtual sources $S_j$, $j=1$ to 1189, were initially set equal to zero and $S_0$ was assigned a value of 1 W. After the first execution of Eq. (3), a set of $F_{i0}$ values were generated, the Born approximation. Equation (5) converted $F_{i0}$ into $S_j$ values for the 1189 virtual sources. Repeating the use of Eq. (3), both the primary and the virtual sources contributed to $F_i$ and Eq. (5) updated the virtual sources. The iterative application of Eqs. (3) and (5) caused the virtual source powers to converge on a final set of stable values. After convergence, one could calculate and sum the contributions of $S_0$ and all 1189 virtual sources to any position of observation using an expression similar to Eq. (3). The primary source and virtual sources were used to generate the fluence rate in a 14 cm×14 cm $x$-$y$ plane at $z=0$ connecting the source, center of the fetal brain, and detector.

Results were expressed as the transport factor $T=F/S_0$ ($cm^{-2}$) so the results are applicable to any source power $S_0$ that might be chosen. Hence, a map of the transport distribution ($T_f$) in the infinite maternal tissue with perturbation by the fetal brain was calculated. The transport distribution ($T_m$) without any fetal brain perturbation of light transport was calculated by considering only the primary source $S_0$.

The execution time for an 1189-sphere simulation of both $T_m$ and $T_f$ using Matlab™ version 5.1 on a Macintosh G3 computer was 378 s for setting up the $T_{ij}$ factors, 14 s to iterate Eqs. (2) and (3) 50 times, and 248 s to output a 40×40 grid map of the results, for a total of 640 s.

### 2.3 Perturbation Model: Air/Tissue Abdominal Boundary

Second, the air/tissue boundary was added at the abdominal surface. This boundary was accomplished by the method of images which places a set of virtual sources outside the surface to meet the boundary condition along the abdominal surface. The boundary condition consists of the relationship between the fluence rate $F_0$ in the tissue at the surface boundary and the outward flux $J$ crossing the surface boundary. At the boundary, the fluence rate $F_0$ equals $2AJ$ where $A$ is $(1+r_{tir})/(1-r_{tir})$ as previously mentioned. The outward flux $J$ across the boundary equals $D(F_1-F_2)/d$ where $F_1$ and $F_2$ are fluence rates at positions one $mfp'$ below and one $mfp'$ above the boundary, respectively, and $d$ is the separation between the $F_1$ and $F_2$ positions, or $2mfp'$. Hence, the boundary condition is

$$\frac{F_0}{2A}=D\frac{F_1-F_2}{d}. \tag{6}$$

To mimic the primary source directed onto the maternal abdomen with an air/tissue boundary, a positive source $S_0$ was placed one $mfp'$ below the surface and a negative source $-S_0$ was placed a distance $(mfp'+4AD)$ above the surface at the position of the true primary source. This pair of real and image sources mimicked an air/tissue boundary following the example of Farrel et al.[10] Additionally, a set of 440 boundary images sources were placed outside the surface every 8.59° in the circumferential and azimuthal directions which covered the entire upper hemisphere associated with the maternal abdominal surface [not all the image sources are shown in Figure 1(b)]. The powers associated with these image sources were adjusted individually to achieve the boundary condition of Eq. (6). The set of sources $S_j$ consisted of the two primary sources, the real positive source $S_1=S_0$ and its negative image $S_2=-S_0$, and the 440 additional boundary image sources $S_3$ to $S_{442}$. The powers of the 440 image sources were iteratively adjusted by a change $\Delta S$

$$\Delta S_i=\frac{\sum_{j=1}^{N} S_j\left[\frac{T_{0ij}}{2A}-\frac{T_{1ij}-T_{2ij}}{d}\right]}{D\frac{T_{b1}-T_{b2}}{d}-\frac{T_{b0}}{2A}} \tag{7}$$

for $i=3-442$. $T_{0ij}$ is the transport factor [similar to Eq. (1)] from the $j$th source to the position on the surface indicated by No. 0 in Figure 2. $T_{1ij}$ is the transport from the $j$th source to the position indicated by No. 1 in Figure 2. $T_{2ij}$ is the transport from the $j$th source to the position indicated by No. 2 in Figure 2. The denominator of Eq. (7) is a constant and $T_{b1}$ is the transport from the $i$th boundary image source to position

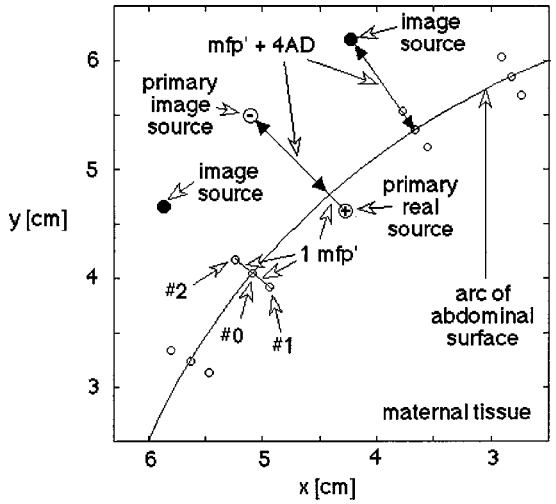


**Fig. 2** Close-up view of model that mimics the air/tissue boundary of Figure 1(b). The primary real source is positive and one $mfp'$ below the surface. The primary image source is negative and located $mpf' + 4AD$ above the surface. A hemisphere of negative boundary image sources are positioned $mpf' + 4AD$ above the surface at 8.59° intervals. Three positions inside, on, and outside the surface are indicated by the labels Nos. 1, 0, and 2, respectively. The transport $T_{1j}$, $T_{0j}$, and $T_{2j}$ from all sources to these positions are used to evaluate the balance between outward flux and fluence rate at the boundary so as to specify the strength of the boundary image sources.

No. 1 in Figure 2 calculated by Eq. (1) where $r_{ij} = 2mfp' + 4AD$. $T_{b2}$ is the transport from the $i$th boundary image source to position No. 2 calculated by Eq. (1) where $r_{ij} = 4AD$. $T_{b0}$ is the transport from the $i$th boundary image source to position No. 0 calculated by Eq. (1) where $r_{ij} = mfp' + 4AD$. The value $\Delta S_i$ was used to update each $j$th boundary image source as follows:

$$S_{j=3-442} = S_{j=3-442} + b\Delta S_{i=1-440}, \tag{8}$$

where $b$ equaled 0.5 to allow only partial updates of $S_i$. Equations (7) and (8) were iterated to allow each boundary image source $S_i$ to converge to its final stable value. The value of $b$ was chosen to avoid instability during the convergence of the boundary image source values.

To calculate the case of no optical perturbation by the fetus, i.e., $\mu_{af} = \mu_{am}$, the set of sources $S_j$ consisted of two primary sources and 440 boundary sources for a total of $N = 442$ sources. Equation (7) summed the numerator over all sources, i.e., $j = 1$ to $N$, and Eq. (8) updated the 440 boundary image sources. To calculate the case of optical perturbation by the fetal brain, i.e., $\mu_{af} > \mu_{am}$, an additional 1189 virtual sources were added to the set of $S_j$ sources, as was described in the previous section for no air/tissue abdominal boundary. There were $N = 2 + 440 + 1189 = 1631$ sources used in the iterative application of Eqs. (3) and (5) for the purpose of allowing the 1189 virtual sources to converge to final values. Iterative application of Eqs. (7) and (8) to update the boundary sources ($j = 3-443$) and application of Eqs. (3) and (5) to update the virtual sources ($j = 444-1631$) allowed all source values to converge to final stable values. The two primary sources and the 440 boundary image sources were used to generate an $x$-$y$ map of the light transport $T_m$ without fetal perturbation. All the primary, boundary image, and virtual sources were used to generate the $x$-$y$ map of the light transport $T_f$ with fetal perturbation.

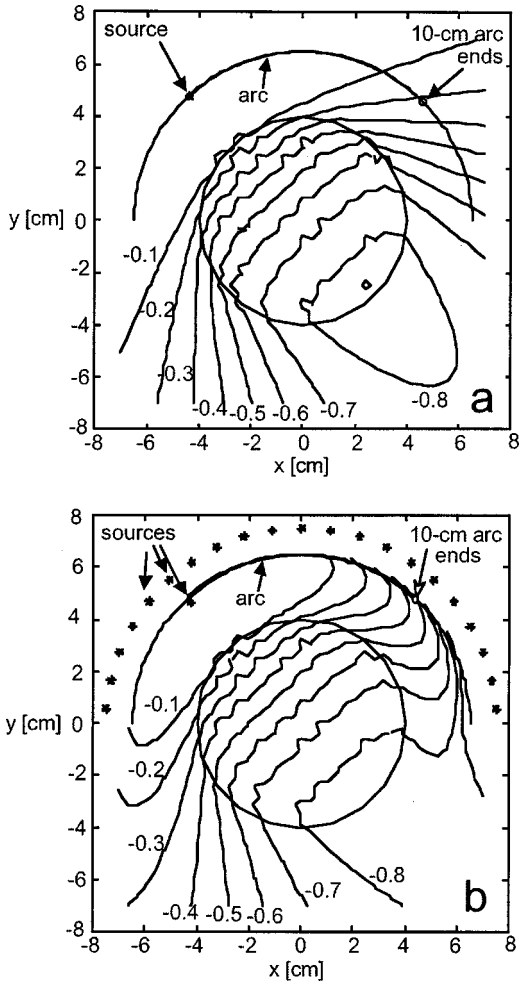


**Fig. 3** Map of the perturbation of light transport caused by the fetal brain. The map shows the fetal perturbation $P$ of optical transport for the $x$-$y$ plane containing the source, brain center, and detector. The isoperturbation curves show the fractional reduction in transport caused by the fetus. For example, the –0.30 curve indicates a 30% reduction in light transport relative to the transport with no fetal incremental absorption. (a) No boundary. (b) With air/tissue boundary.

The execution time for the 1631-source simulation of both $T_m$ and $T_f$ using Matlab™ version 5.1 on a Macintosh G3 computer was 437 s for setting up Eqs. (3)–(8) for the iterative calculations, 17 s to accomplish 50 iterations, and 388 s to output a 40×40 grid map of the results, for a total of 842 s.

## 3 Results

The $x$-$y$ maps of $T_m$ (no fetal perturbation) and $T_f$ (with fetal perturbation) were used to generate a perturbation map where perturbation $P$ is defined

$$P = \frac{T_f - T_m}{T_m}. \tag{9}$$

Figure 3 shows the map of $P$ in the $x$-$y$ plane containing

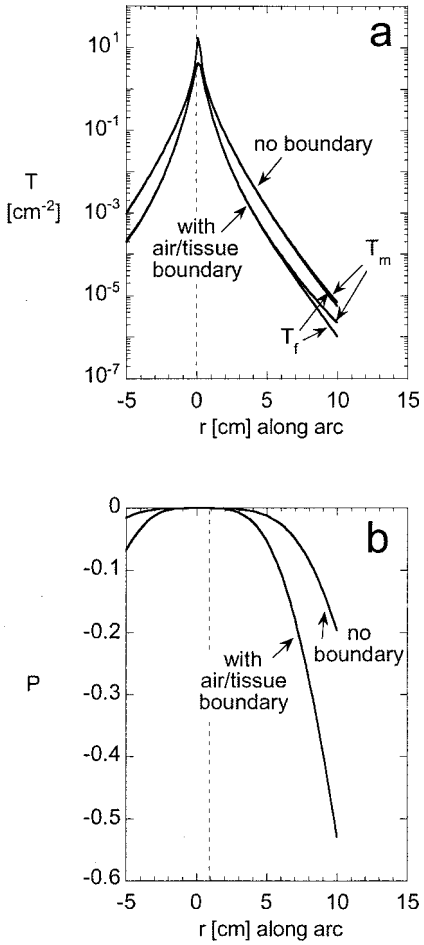


**Fig. 4** (a) Optical transport versus position along the abdominal arc, with ($T_f$) and without ($T_m$) optical perturbation by the fetal brain. (b) Fetal perturbation ($P$) of optical transport. Both figures show the two cases of with and without an air/tissue boundary.

the source, fetal brain center, and detector. Figure 3(a) shows the map for the case of an infinite maternal tissue with no air/tissue boundary. Figure 3(b) shows the case of an air/tissue boundary. The curves of Figure 3 are isoperturbation contours. For example, the contour labeled $-0.3$ indicates that the presence of the fetal incremental absorption has caused a 30% reduction in the light transport relative to the absence of fetal incremental absorption. Notice how the fetal brain casts a shadow of perturbation. In contrast, the perturbation in the intervening space between source and fetus is negligible. In Figure 3(b), the effect of the air/tissue boundary is to curl the isoperturbation lines closer to the source thereby increasing the strength of the fetal perturbation at a fixed detector position.

Figure 4 shows how the fetal brain perturbs the light field along the 10 cm arc associated with the maternal abdominal surface. A pair of curves for both the case of an infinite maternal tissue with no boundary and the case of an air/tissue boundary are shown. In Figure 4(a) for each case, the transport to detectors along the arc is shown as a pair of curves, $T_f$ and $T_m$. The magnitude of transport falls orders of magnitude as the detector moves further from the source along the abdominal arc. The presence of the fetal brain's incremental absorption causes a decrease in the transport. This fetal perturbation is more marked for the case of an air/tissue boundary. In Figure 4(b), the perturbation $P$ along the arc is plotted. The perturbation is minimal while the detector is close to the source because transport is dominated by reflectance from the maternal tissue layer above the fetus. Once the detector moves past the midline (vertical dashed line) of the abdomen, transport becomes more sensitive to the fetal brain. Again, the presence of an air/tissue boundary increases the magnitude of the fetal perturbation of the optical field. Without a boundary, photons which never pass through the fetal head can still return to the detector. With the boundary, these photons escape the maternal tissues which increases the fraction of collected photons that pass through the fetus.

## 4 Discussion

The practical implementation of transabdominal fetal oximetry will likely require measurements of $T_f$ along the abdominal arc. Close to the source $T_m$ approximately equals $T_f$ and measurements close to the source will therefore also characterize the background behavior of the maternal tissues. This behavior can be extrapolated to predict expected $T_m$ measurements at large source-detector distances. The deviation of actual measurements of $T_f$ distant from the source from the predicted $T_m$ measurements can be attributed to the influence of the fetal brain. Ultrasound measurements of the maternal thickness above the fetal head will likely be critical to specifying the true geometry of the problem and enabling interpretation of the optical measurements across the abdomen.

The difference signal $\Delta T = T_m - T_f$ is strongest near the source. However, the magnitude of the near-source $T_f$ signal forces the dynamic range of the detection system to cover the large $T_f$ signal and the $\Delta T$ is likely to fall below the dynamic range of measurement. However, measurements far from the source will greatly decrease the magnitude of the $T_f$ signal which allows the dynamic range to discern $\Delta T$. The perturbation $P$ is pertinent to the measurement of $\Delta T$ with a detector whose dynamic range must measure $T_f$. Figure 4(b) suggests that $P$ is maximal at the largest source-detector separation possible. The ultimate noise floor of the detector at maximum gain will determine the maximum source-detector separation that is useful.

In summary, the preliminary modeling of this paper indicates that the fetal brain will decrease transabdominal measurements of near-infrared light transport by about 10% at a 6.0 cm source-detector separation and by about 53% at a 10 cm separation. While the challenge of specifying the maternal baseline is significant, the modeling suggests that there is an opportunity to sense the fetal brain with transabdominal optical measurements. Using multiple wavelengths of near-infrared light would allow fetal oximetry.

## References

1. N. Ramanujam, H. Long, M. Rode, I. Forouzan, M. Moregan, and B. Chance, ''Antepartum, transabdominal near infrared spectgroscopy: Feasibiligy of measuring photon mibgration through the fetal heat in utero,'' *J. Mater. Fetal Med.* **8**, 275–288 (1999).
2. M. A. O'Leary, D. A. Boas, B. Chance, and A. G. Yodh, ''Refraction of diffuse photon density waves,'' *Phys. Rev. Lett.* **69**, 2658–2661 (1992).
3. R. L. Barbour, H. L. Graber, Y. Wang, J. Chang, and R. Aronson, ''A

perturbation approach for optical diffusion tomography using continuous-wave and time-resolved data,'' in *Medical Optical Tomography: Functional Imaging and Monitoring*, G. Mueller et al., Ed., *SPIE Institutes*, **IS11**, 87–120, SPIE, Bellingham, WA (1993).
4. S. Feng, F-A Zeng, and B. Chance, ''Perturbation theory of photon migration in the presence of a single defect,'' in *OSA Proceedings on Advances in Optical Imaging and Photon Migration*, **21**, 217–228, R. R. Alfano, Ed., Optical Society of America, Washington, DC (1994).
5. S. L. Jacques, M. R. Ostermeyer, L. Wang, and A. H. Hielscher, ''Effects of sources, boundaries, and heterogeneities on photon migration,'' in *OSA Proceedings on Advances in Optical Imaging and Photon Migration*, **21**, 83–87, R. R. Alfano, Ed., Optical Society of America, Washington, DC (1994).
6. M. R. Ostermeyer and S. L. Jacques, ''Perturbation theory for diffuse light transport in complex biological tissues,'' *J. Opt. Soc. Am. A* **14**, 255–261 (1997).
7. L. O. Svaasand and R. Ellingsen, ''Optical properties of human brain,'' *Photochem. Photobiol.* **38**, 293–299 (1983).
8. N. Ramanujam, G. Vishnoi, A. Hielscher, M. Rode, I. Forouzan, and B. Chance, ''Photon migration through fetal head *in utero* using continuous wave, near infrared spectroscopy: Clinical and experimental model studies,'' *J. Biomed. Opt.* **5**(2), 173–184 (2000).
9. G. Vishnoi, A. H. Hielscher, N. Ramanujam, and B. Chance, ''Photon migration through fetal head *in utero* using continuous wave, near infrared spectroscopy: Development and evaluation of experimental and numerical models,'' *J. Biomed. Opt.* **5**(2), 163–172 (2000).
10. T. J. Farrel, M. S. Patterson, and B. Wilson, ''A diffusion theory model of spatially resolved, steady-state diffuse reflectance for the noninvasive determination of tissue optical properties *in vivo*,'' *Med. Phys.* **19**, 881–888 (1992).